Unmanned Systems, Vol. 14, No. 1 (2026) 227–238

DOI: 10.1142/S2301385025500918

UNMANNED SYSTEMS
https://www.worldscientific.com/worldscinet/us

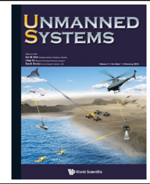


# Robust Formation Control of Quadrotor UAVs: A Fully-Actuated Control Approach

Zhihao Liu *, Peng Li †

*School of Mechanical Engineering and Automation*
*Harbin Institute of Technology (Shenzhen) 518055, P. R. China*

In this work, a fully actuated system (FAS) control scheme for the quadrotor UAV formation is designed. Deploying the FAS techniques, two controllers are designed for position and angle tracking so that the UAV formation is driven along the given trajectory with enhanced internal stability. Considering the scenario where the environment disturbances and actuator faults affect UAV systems, an extended state observer (ESO) is designed to estimate the uncertainty. Subsequently, the effect of the fault and uncertainty is compensated in the FAS controller to enhance the accuracy. As a result, the proposed formation coordination controller ensures that the UAV team completes the desired flight mission. According to the simulation results, the proposed method is more accurate and robust against the disturbance and fault with the accurate estimation compared with traditional methods.

*Keywords*: Quadrotor UAV formation; fully actuated system control; fault identification; extended state observer.

## 1. Introduction

Quadrotor unmanned aerial vehicle (UAV) has been widely used in military and civilian fields. Multi-UAV formation control is a fundamental research topic in the field of UAV collaborative control. Presently, the control approaches of UAV formation mainly include the leader–follower method [1], the virtual structure method [2], the behavior-based method [3], and the artificial potential field method [4]. Additionally, drones may be affected by external environmental disturbances or internal component faults while performing tasks. Therefore, it is of practical significance to consider both external environmental disturbances and actuator faults in UAV formation problems. In [5], the high-order consistency theory is applied in UAV formation flight control strategy, simplifying the nonlinear mathematical model of the quadrotor UAV. In [6, 7], the control algorithms of UAV time-varying formation are designed based on consistency theory and are verified on a quadrotor hardware platform. The consensus formation has been extensively studied. However, during maintaining formation, there is still a large gain convergence oscillation in the linear consensus algorithm. A case of follower UAV actuator faults are is considered in [8] and the authors proposed a distributed fault-tolerant formation control strategy based on the virtual leader. A distributed fault-tolerant formation control strategy based on adaptive sliding mode was proposed in [9] to achieve rapid formation recovery in the event of UAV fault. In [10], a disturbance observer was designed to address the modeling coupling factors and external environmental disturbances to achieve formation stability. However, the above literature did not consider both UAV failures and the external environmental disturbances simultaneously.

In recent years, the fully actuated system technique [11] has introduced a new theoretical approach for the control field, characterized by its high convergence rate and simple parameter design. A trajectory tracking controller based on a second-order fully-actuated system model for a six-degree-of freedom manipulator with uncertainties is designed in [12]. In [13], an attitude control of a flexible aerocraft is transformed into a problem of time-varying nonlinear control through fully actuated system technique. Furthermore, a

Received 23 July 2024; Accepted 27 November 2024; Published 22 January 2025. This paper was recommended for publication in its revised form by editorial board member, Shiyu Zhao.
Email Addresses: *liuzhihaotina@163.com, †lipeng2020@hit.edu.cn
† Corresponding author.

fully auactuated system model for the six degree-of-freedom spacecraft motion is derived and a tracking controller based on FAS approach is designed in [14]. However, few designed the FAS controllers for UAV formation considering external disturbances and actuator faults simultaneously. Therefore, combined with the leader–follower formation control strategy, this paper designs a fully actuated system control approach based on the expanded state observer to ensure robust control of UAV formation. There exist some problems using traditional methods. For example, the sliding mode control has fluctuation; the adaptive control may not guarantee global stability; the linear consensus algorithm leaves a large gain convergence oscillation. Fortunately, the FAS algorithm has no such problems. Liu and Li [15] has proofed that FAS converges faster than SMC with less steady-state error. However, it requires accurate knowledge of system dynamics resulting in that it is not robust to large uncertainty [14]. Thus one can combine some techniques such as the extend state observer to estimate and compensate the uncertainty for better control performance.

The main contributions of this paper are as follows:

(1) The under actuated UAV system with coupled terms is transformed into a fully actuated one through the fully actuated theorem, obtaining the direct input and solving the actual input according to the dynamics. The proposed scheme ensures the stable convergence and simplifies the design of the controller.
(2) The combination of the FAS controller and the ESO enhances the internal stability and robustness, as verified by extensive numerical experiments.
(3) Compared with other traditional methods, the proposed has a simpler form, less fluctuation, and a higher convergence rate, with guaranteed global convergence.

The rest of this paper is arranged as follows: Sec. 2 establishes a dynamic model of the UAV with external disturbances and actuator faults and introduces the fully actuated system theory. Section 3 discusses controller and extend state observer designs for position and attitude layers with the robustness analysis and stability proof. Specific examples are given in Sec. 4 for simulation verification. Section 5 summarizes the results and proposes further research directions.

## 2. Preliminaries

### 2.1. *Dynamic model of UAV*

Suppose the quadcopter drone is a rigid body with the geometric center consistent with the center of mass. The UAV dynamic coordinate system model is shown in


Fig. 1. Four rotor propellers.

Fig. 2. The roll angular $\phi$, the pitch angular $\theta$, and the yaw angular $\psi$ denote the rotation angles around the $x_b$, $y_b$, and $z_b$ axes, respectively, which normally range within $(-\frac{\pi}{2}, \frac{\pi}{2})$. As in Fig. 1, $\tau_k (k \in [1, 4])$ represents the combined thrust or force provided by the $k$th motor. They can be combined into four moments as [16]

$$U_{1,i} = \tau_1 + \tau_2 + \tau_3 + \tau_4, \quad U_{2,i} = -\tau_2 + \tau_4,$$
$$U_{3,i} = -\tau_1 + \tau_3, \quad U_{4,i} = -\tau_1 + \tau_2 - \tau_3 + \tau_4,$$

where $U_{1,i}$ represents the lift force of the $i$th UAV; $U_{r,i}$ $(r \in [2, 4])$ represents the roll, pitch or yaw force, respectively.

The control input of the $i$th quadcopter drone under actuator fault is as follows:

$$U_{ra,i} = U_{r,i} + f_{r,i}, \quad (r = 1, 2, 3, 4),$$

where $r$ represents the torques with $r = 1$ for the lift one and $r = 2, 3, 4$ for the attitudes ones; $U_{ra,i}$ is the actual control input; $U_{r,i}$ is the designed input; $f_{r,i}$ is the deviation failure factor of the $r$th combined moment, and actuator fault occurs when $f_{r,i} \neq 0$.

Consider a multi-UAV system consists of $N (N > 1)$ UAVs with each one being affected by environmental disturbance and actuator fault. The dynamics of the $i$th

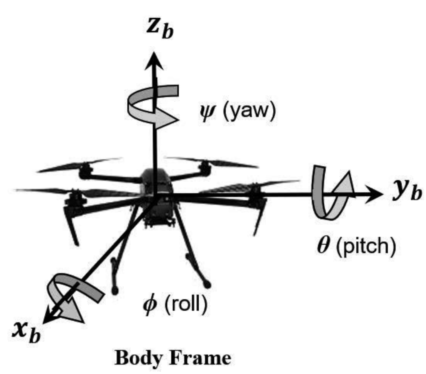


Fig. 2. Coordinate system of the quadrotor.

UAV [17] is expressed as

$$\begin{cases} \ddot{x}_i = \dfrac{\cos\phi_i \sin\theta_i \cos\psi_i + \sin\phi_i \sin\psi_i}{m_i} U_{1a,i} \\ \qquad - \dfrac{k_{x,i}}{m_i}\dot{x}_i + d_{x,i}, \\ \ddot{y}_i = \dfrac{\cos\phi_i \sin\theta_i \sin\psi_i - \sin\phi_i \cos\psi_i}{m_i} U_{1a,i} \\ \qquad - \dfrac{k_{y,i}}{m_i}\dot{y}_i + d_{y,i}, \\ \ddot{z}_i = \dfrac{\cos\phi_i \cos\theta_i}{m_i} U_{1a,i} - g - \dfrac{k_{z,i}}{m_i}\dot{z}_i + d_{z,i}, \\ \ddot{\phi}_i = \dfrac{J_{y,i} - J_{z,i}}{J_{x,i}}\dot{\theta}_i\dot{\psi}_i + \dfrac{U_{2a,i}}{J_{x,i}} d_i - \dfrac{k_{\phi,i}}{J_{x,i}}\dot{\phi}_i + d_{\phi,i}, \\ \ddot{\theta}_i = \dfrac{J_{z,i} - J_{x,i}}{J_{y,i}}\dot{\phi}_i\dot{\psi}_i + \dfrac{U_{3a,i}}{J_{y,i}} d_i - \dfrac{k_{\theta,i}}{J_{y,i}}\dot{\theta}_i + d_{\theta,i}, \\ \ddot{\psi}_i = \dfrac{J_{x,i} - J_{y,i}}{J_{z,i}}\dot{\theta}_i\dot{\phi}_i + \dfrac{U_{4a,i}}{J_{z,i}} - \dfrac{k_{\psi,i}}{J_{z,i}}\dot{\psi}_i + d_{\psi,i}, \end{cases} \tag{1}$$

where $x_i$, $y_i$ and $z_i$ are the positions of the $i$th UAV in the inertial coordinate system; $\phi_i$, $\theta_i$ and $\psi_i$ are the attitude angles. $J_{x,i}$, $J_{y,i}$ and $J_{z,i}$ are the moments of inertia around $x$-, $y$- and $z$-axes; $g$ is the acceleration due to gravity; $k_{x,i}$, $k_{y,i}$ and $k_{z,i}$ are the air resistance coefficients; $k_{\phi,i}$, $k_{\theta,i}$ and $k_{\psi,i}$ are aerodynamic drag coefficients; $d_{k,i}(k = x, y, z, \phi, \theta, \psi)$ is environmental disturbance; $d_i$ is the distance between the center of the $i$th drone and the center of its rotor; $m_i$ is the mass of the $i$th UAV.

For convenience, we define the disturbance and fault vectors in position and attitude layers as

$$\boldsymbol{\sigma}_{p,i} = \begin{bmatrix} b_{x,i}f_{1,i} + d_{x,i} \\ b_{y,i}f_{1,i} + d_{y,i} \\ b_{z,i}f_{1,i} + d_{z,i} \end{bmatrix},$$

$$\boldsymbol{\sigma}_{a,i} = \begin{bmatrix} b_{\phi,i}f_{2,i} + d_{\phi,i} \\ b_{\theta,i}f_{3,i} + d_{\theta,i} \\ b_{\psi,i}f_{4,i} + d_{\psi,i} \end{bmatrix},$$

with

$$\begin{bmatrix} b_{x,i} \\ b_{y,i} \\ b_{z,i} \\ b_{\phi,i} \\ b_{\theta,i} \\ b_{\psi,i} \end{bmatrix} = \begin{bmatrix} \dfrac{\cos\phi_i \sin\theta_i \cos\psi_i + \sin\phi_i \sin\psi_i}{m_i} \\ \dfrac{\cos\phi_i \sin\theta_i \sin\psi_i - \sin\phi_i \cos\psi_i}{m_i} \\ \dfrac{\cos\phi_i \cos\theta_i}{m_i} \\ d_i/J_{x,i} \\ d_i/J_{y,i} \\ 1/J_{z,i} \end{bmatrix}.$$

We assume that the total uncertainty with disturbance and fault is a bounded slow variable function and satisfies $\lim_{t\to\infty} \dot{\boldsymbol{\sigma}}_{p,i}(t) = 0$ and $\lim_{t\to\infty} \dot{\boldsymbol{\sigma}}_{a,i}(t) = 0$ [18]. The large and unbounded situation will be include in future work.

### 2.2. *Fully actuated system theory*

Consider a second-order dynamic system

$$E\ddot{x} = f(x, \dot{x}, t) + B(x, \dot{x}, t)u, \tag{2}$$

where $E \in R^{n\times n}$ is a matrix of constants that can be singular; $x \in R^{n\times 1}$ is the state of the system; $f(x, \dot{x}, t) \in R^{n\times 1}$ is a continuous vector function of state variables, their derivatives and time; $B(x, \dot{x}, t) \in R^{n\times n}$ is the matrix of coefficients; $u \in R^{n\times 1}$ is the control input. If the control distribution matrix $B$ satisfies

$$\det B(x, \dot{x}, t) \neq 0, \quad \forall x,\ \dot{x} \in R^{n\times 1},\ t \geq 0,$$

then the system (2) is fully actuated. The following linear and constant closed-loop system is obtained

$$E\ddot{x} + A_1\dot{x} + A_0x = v,$$

through selecting suitable constant matrices $A_1$, $A_2 \in R^{n\times n}$, which produces the control law as

$$u = -B^{-1}(A_1\dot{x} + A_0x + f - v),$$

where $v \in R^{n\times 1}$ is the designed input of the closed-loop system. Especially, let $E = I_n$ and $v = 0_{n\times 1}$. Then the system (2) is transformed into

$$\ddot{x} = -A_1\dot{x} - A_0x.$$

Define $z_1 = x$, $z_2 = \dot{x}$. The target system is

$$\dot{z} = \begin{bmatrix} \dot{z}_1 \\ \dot{z}_2 \end{bmatrix} = \begin{bmatrix} \mathbf{0} & I \\ -A_0 & -A_1 \end{bmatrix} \begin{bmatrix} z_1 \\ z_2 \end{bmatrix} = Az. \tag{3}$$

Select $A_1$ and $A_0$ properly so that the matrix $A$ in (3) can be Hurwitz. Then the system is stable consequently, which means that one can expect that the states of (3) converge to zero finally.

It is worth noting that there is difference between FAS control and the feedback linearization control, since the FAS approach directly designs parameters for the whole high-order systems while the feedback linearization just designs for the derivatives of the states. Although, for first-order system, they are the same. For second-order and higher systems, the feedback linearization cannot ensure both the states and their derivatives converge to zero while FAS can according to Hurwitz criterion. For instance, considering a second-order system as in (2), the following system can be obtained through feedback linearization:

$$E\ddot{x}' = -C\dot{x}',$$

where $C$ is a constant matrix to be designed. Then one can only conclude that $\dot{x}'$ and $\ddot{x}'$ will converge to zero, however without the convergence guarantee of $x'$, since the target system is

$$\dot{z}' = \begin{bmatrix} \dot{z}'_1 \\ \dot{z}'_2 \end{bmatrix} = \begin{bmatrix} \mathbf{0} & I \\ \mathbf{0} & -C \end{bmatrix} \begin{bmatrix} z'_1 \\ z'_2 \end{bmatrix} = A'z',$$

where $z'_1 = x'$, $z'_2 = \dot{x}'$; the matrix $A'$ cannot be Hurwitz as $\det(A') = 0$. This may cause the error accumulation on $x'$. High-order fully actuated system approach can avoid the problem since it guarantees the convergences of $x$, $\dot{x}$ and $\ddot{x}$ as in (3).

Moreover, the parameter design through FAS approach is more flexible and intuitive. However, FAS technique required accurate knowledge of system dynamics. Although it is robust to small modeling errors, it is not suitable for large uncertainty, for example, in the scenario where it lacks the knowledge of system model. Consequently the closed-loop system will be affected by the uncertainty. On the other hand, a disturbance observer can be instrumental in enhancing the closed-loop control performance.

**Notations:** $\|\cdot\|$ defines the norm of vectors; $\mathbf{0}$ represents zero matrix; $I$ is identity matrix; and $\lambda_{\min}$ and $\lambda_{\max}$ represent the largest and smallest eigenvalues of one matrix, respectively.

## 3. Main Results

The formation control problem is transformed into a velocity and trajectory tracking problem under a leader–follower framework. One virtual leader is considered to provide the given trajectory. Then one UAV follows it and rest of each UAV has one corresponding leader. That is, each UAV may have multiple followers but only follows one leader itself. As shown in Fig. 3, for each pair of leader–follower-, set a stationary relative position offset $[\Delta x_{ij}, \Delta y_{ij}, \Delta z_{ij}]$ to obtain the desired formation.

We make some assumptions about the leader–follower system:

(1) There is no communication delay between the leader and follower.
(2) Each robot can detect its own pose, velocity and acceleration.
(3) The leader can transmit its information mentioned above to each of its followers through communication.

The formation goal is to obtain trajectory consistency. Firstly, the desired trajectory of the whole UAV team is from one virtual leader following a given trajectory. Then the team follows the trajectory according to the leader–follower strategy. The control inputs are the four torques $U_r(r \in [1,4])$ of UAV determining the position and attitude of each drone.

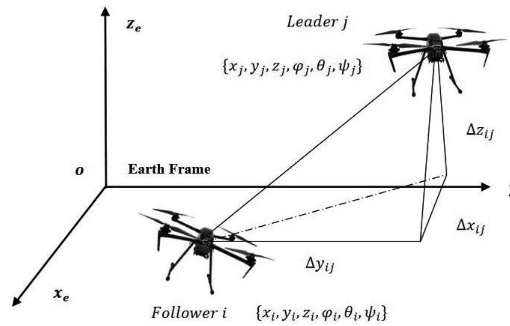


Fig. 3. The relative kinematics of the leader–follower.

Regarding the strong coupled dynamics as in (1), the position layer and the attitude layer cannot be combined into an overall second-order model to design the control law [16]. Therefore, the control is considered in position and attitude layers, respectively. Also the ESOs are designed for position and attitude control, respectively. In general, the attitude changes slowly and moderately, so that the effects of the angle variation on position control can be reasonably ignored. The position control torque $U_{1,i}$ is obtained based on FAS under the leader–follower tracking framework. And the ESO is proposed to estimate the effects of actuator fault and the disturbance, so that it can be compensated in the controller. Based on the dynamics model (1), the desired attitude angles can be uniquely determined with $U_{1,i}$ solved and compensation term $\hat{\boldsymbol{\sigma}}_{a,i}$ by ESO. Then with the desired attitudes, we design the direct inputs in attitude control layer deploying FAS technique and obtain the control torques $U_{r,i}(r \in [2,4])$ according to (1). With the four torques solved, UAVs' position and attitude can be maneuvered. The uncertainties caused by disturbance and fault are estimated and compensated through ESO that guarantees the robustness of the system. The flowchart of the algorithm applied is Fig. 4.

### 3.1. *Position control*

Consider the $i$th UAV and its leader-the $j$th UAV. Define the position error $\boldsymbol{e}_{p,i}$ and the vector $\boldsymbol{z}_{p,i}$ as

$$\boldsymbol{e}_{p,i} = \begin{bmatrix} x_i - x_j - \Delta x_{ij} \\ y_i - y_j - \Delta y_{ij} \\ z_i - z_j - \Delta z_{ij} \end{bmatrix},$$

$$\boldsymbol{z}_{p,i} = \begin{bmatrix} \boldsymbol{e}_{p,i} \\ \dot{\boldsymbol{e}}_{p,i} \end{bmatrix}.$$

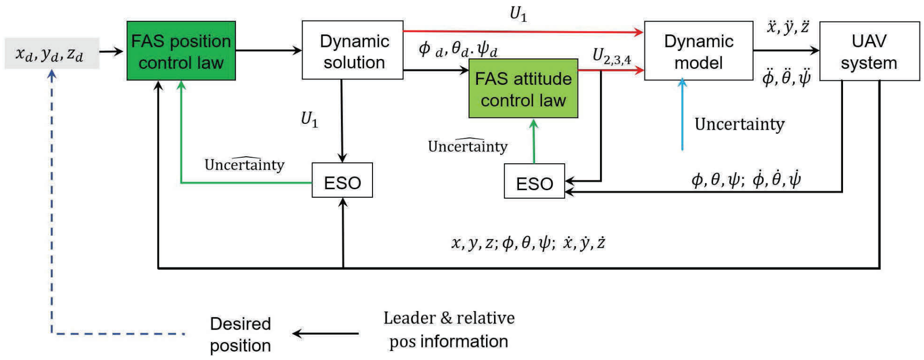


Fig. 4. The flowchart of this work.

The second derivative of position error system is

$$\ddot{\boldsymbol{e}}_{p,i} = \boldsymbol{a}_i - \boldsymbol{a}_j + \boldsymbol{\sigma}_{p,i}, \tag{4}$$

where $\boldsymbol{a}_i$ and $\boldsymbol{a}_j$ are the theoretical linear accelerations of the $i$th UAV and $j$th UAV, respectively. As in (4), the coefficient matrix of $\boldsymbol{a}_i$ is identity matrix whose determinant is $1 \neq 0$. Therefore, the system (4) is fully actuated. The error dynamics can be expressed as

$$\dot{\boldsymbol{z}}_{p,i} = \begin{bmatrix} \dot{\boldsymbol{e}}_{p,i} \\ \ddot{\boldsymbol{e}}_{p,i} \end{bmatrix} = \begin{bmatrix} \dot{x}_i - \dot{x}_j \\ \dot{y}_i - \dot{y}_j \\ \dot{z}_i - \dot{z}_j \\ \ddot{x}_i - \ddot{x}_j \\ \ddot{y}_i - \ddot{y}_j \\ \ddot{z}_i - \ddot{z}_j \end{bmatrix} = \begin{bmatrix} \boldsymbol{v}_i - \boldsymbol{v}_j \\ \boldsymbol{a}_i - \boldsymbol{a}_j \end{bmatrix} + \begin{bmatrix} \boldsymbol{0} \\ \boldsymbol{\sigma}_{p,i} \end{bmatrix}, \tag{5}$$

where $\boldsymbol{v}_i$ and $\boldsymbol{v}_j$ are the linear velocities of the $i$th UAV and $j$th UAV, respectively. The total uncertainty term $\boldsymbol{\sigma}_{p,i}$ is estimated through ESO as follows.

For position control layer, define the variables as

$$\begin{aligned} \boldsymbol{\nu}_{1,i} &= [x_i \quad y_i \quad z_i]^T, \\ \boldsymbol{\nu}_{2,i} &= [\dot{x}_i \quad \dot{y}_i \quad \dot{z}_i]^T, \\ \boldsymbol{\nu}_{3,\boldsymbol{i}} &= \boldsymbol{\sigma}_{p,i} - \begin{bmatrix} k_{x,i} \\ k_{y,i} \\ k_{z,i} \end{bmatrix} \boldsymbol{\nu}_{2,i}/m_i - \begin{bmatrix} 0 \\ 0 \\ g \end{bmatrix}. \end{aligned} \tag{6}$$

where $\boldsymbol{\nu}_{3,\boldsymbol{i}} = [\ddot{x}_i \quad \ddot{y}_i \quad \ddot{z}_i]^T - [b_{x,i} \quad b_{y,i} \quad b_{z,i}]^T U_{1,i}$ is the sum of the uncertainty and the known resistance. The state equation of position layer can be obtained from (1)

$$\begin{cases} \dot{\boldsymbol{\nu}}_{1,i} = \boldsymbol{\nu}_{2,i}, \\ \dot{\boldsymbol{\nu}}_{2,i} = \begin{bmatrix} b_{x,i} \\ b_{y,i} \\ b_{z,i} \end{bmatrix} U_{1,i} + \boldsymbol{\nu}_{3,i}, \\ \dot{\boldsymbol{\nu}}_{3,i} = \boldsymbol{\rho}_{p,i}, \end{cases}$$

where $\boldsymbol{\rho}_{p,i}$ is the derivative of $\boldsymbol{\nu}_{3,\boldsymbol{i}}$. Let the input be $\boldsymbol{\nu}_{1,i} = [x_i, y_i, z_i]^T$. Define the following extended state observer:

$$\begin{cases} \dot{\hat{\boldsymbol{\nu}}}_{1,i} = \hat{\boldsymbol{\nu}}_{2,i} + \dfrac{\alpha_{1,i}}{\varepsilon_i}(\boldsymbol{\nu}_{1,i} - \hat{\boldsymbol{\nu}}_{1,i}), \\ \dot{\hat{\boldsymbol{\nu}}}_{2,i} = \begin{bmatrix} b_{x,i} \\ b_{y,i} \\ b_{z,i} \end{bmatrix} U_{1,i} + \hat{\boldsymbol{\nu}}_{3,i} + \dfrac{\alpha_{2,i}}{\varepsilon_i^2}(\boldsymbol{\nu}_{1,i} - \hat{\boldsymbol{\nu}}_{1,i}), \\ \dot{\hat{\boldsymbol{\nu}}}_{3,i} = \dfrac{\alpha_{3,i}}{\varepsilon_i^3}(\boldsymbol{\nu}_{1,i} - \hat{\boldsymbol{\nu}}_{1,i}), \end{cases}$$

where $\hat{\boldsymbol{\nu}}_{1,i}$, $\hat{\boldsymbol{\nu}}_{2,i}$ and $\hat{\boldsymbol{\nu}}_{3,i}$ are the estimates of position state variables $x_i, y_i, z_i$, their derivatives and the uncertainty term $\boldsymbol{\nu}_{3,i}$, respectively; $\alpha_{k,i}(k = 1, 2, 3)$ and $\varepsilon_i$ are predetermined positive constants.

**Lemma 3.1.** *For a single-input linear system $\dot{X} = AX + BU$, if $A$ is a Hurwitz matrix and $U$ satisfies $\lim_{t \to \infty} U(t) = 0$, then the system is asymptotic stable [19].*

The error states and its dynamics follow that

$$\begin{aligned} \dot{\varsigma}_{p,i} &= \begin{bmatrix} \dot{\hat{\boldsymbol{\nu}}}_{1,i} - \dot{\boldsymbol{\nu}}_{1,i} \\ \dot{\hat{\boldsymbol{\nu}}}_{2,i} - \dot{\boldsymbol{\nu}}_{2,i} \\ \dot{\hat{\boldsymbol{\nu}}}_{3,i} - \dot{\boldsymbol{\nu}}_{3,i} \end{bmatrix} = \begin{bmatrix} -\dfrac{\alpha_{1,i}}{\varepsilon_i} I & I & \boldsymbol{0} \\ -\dfrac{\alpha_{2,i}}{\varepsilon_i^2} I & \boldsymbol{0} & I \\ -\dfrac{\alpha_{3,i}}{\varepsilon_i^3} I & \boldsymbol{0} & \boldsymbol{0} \end{bmatrix} \varsigma_{p,i} + \begin{bmatrix} \boldsymbol{0} \\ \boldsymbol{0} \\ I \end{bmatrix} \boldsymbol{\rho}_{p,i} \\ &= G_{p,i}\varsigma_{p,i} + H_{p,i}\boldsymbol{\rho}_{p,i}, \end{aligned} \tag{7}$$

where

$$G_{p,i} = \begin{bmatrix} -\frac{\alpha_{1,i}}{\varepsilon_i} I & I & \boldsymbol{0} \\ -\frac{\alpha_{2,i}}{\varepsilon_i^2} I & \boldsymbol{0} & I \\ -\frac{\alpha_{3,i}}{\varepsilon_i^3} I & \boldsymbol{0} & \boldsymbol{0} \end{bmatrix}, \quad \varsigma_{p,i} = \begin{bmatrix} \hat{\boldsymbol{\nu}}_{1,i} - \boldsymbol{\nu}_{1,i} \\ \hat{\boldsymbol{\nu}}_{2,i} - \boldsymbol{\nu}_{2,i} \\ \hat{\boldsymbol{\nu}}_{3,i} - \boldsymbol{\nu}_{3,i} \end{bmatrix},$$

$$H_{p,i} = \begin{bmatrix} \boldsymbol{0} \\ \boldsymbol{0} \\ I \end{bmatrix}.$$

**Assumption 3.2.** The uncertainty term $\boldsymbol{\nu}_{3,i}$ is a bounded slowly-varying variable function and satisfies $\lim_{t\to\infty}\dot{\boldsymbol{\nu}}_{3,i}(t) = \lim_{t\to\infty}\boldsymbol{\rho}_{p,i}(t) = 0$ [18].

By choosing the parameters $\alpha_{1,i}$, $\alpha_{2,i}$, $\alpha_{3,i}$ and $\varepsilon_i$ appropriately, one can make the matrix $G_{p,i}$ Hurwitz. Then based on Lemma 3.1 and Assumption 3.2, the extended state observer asymptotically converges to its true value, which guarantees

$$\lim_{t\to\infty}\hat{\boldsymbol{\nu}}_{3,i} = \boldsymbol{\nu}_{3,i}. \tag{8}$$

Then according to (6), the observed value and the known dynamics, the acceleration compensation term is

$$\hat{\boldsymbol{\sigma}}_{p,i} = \hat{\boldsymbol{\nu}}_{3,i} + \begin{bmatrix} k_{x,i} \\ k_{y,i} \\ k_{z,i} \end{bmatrix} \boldsymbol{\nu}_{2,i}/m_i,$$

directly using the original value $\boldsymbol{\nu}_{2,i} = [\dot{x}_i,\ \dot{y}_i,\ \dot{z}_i]^T$ since it is known by UAV itself according to our previous assumptions. Therefore with (8), define $\boldsymbol{\delta}_{p,i} = \boldsymbol{\sigma}_{p,i} - \hat{\boldsymbol{\sigma}}_{p,i}$ as the observe error vector. It satisfies

$$\lim_{t\to\infty}\|\boldsymbol{\delta}_{p,i}\| = 0. \tag{9}$$

With the estimation from ESO, choose two suitable matrices $A_0$, $A_1 \in R^{3\times3}$ and design the linear acceleration as

$$\boldsymbol{a}_i = \boldsymbol{a}_j - A_1\dot{\boldsymbol{e}}_{p,i} - A_0\boldsymbol{e}_{p,i} - \hat{\boldsymbol{\sigma}}_{p,i}. \tag{10}$$

The system (5) is transformed into

$$\dot{\boldsymbol{z}}_{p,i} = \begin{bmatrix} \mathbf{0} & I \\ -A_0 & -A_1 \end{bmatrix}\begin{bmatrix} \boldsymbol{e}_{p,i} \\ \dot{\boldsymbol{e}}_{p,i} \end{bmatrix} + \begin{bmatrix} \mathbf{0} \\ \boldsymbol{\delta}_{p,i} \end{bmatrix}, \tag{11}$$

where the coefficient matrix can be Hurwitz by suitably choosing $A_0$ and $A_1$. According to dynamics (1), the linear acceleration $\boldsymbol{a}_i$ satisfies the constraint that

$$\boldsymbol{a}_i = \begin{bmatrix} \dfrac{\cos\phi_i\sin\theta_i\cos\psi_i + \sin\phi_i\sin\psi_i}{m_i}U_{1a,i} \\ -\dfrac{k_{x,i}}{m_i}\dot{x}_i + d_{x,i} \\ \dfrac{\cos\phi_i\sin\theta_i\sin\psi_i - \sin\phi_i\cos\psi_i}{m_i}U_{1a,i} \\ -\dfrac{k_{y,i}}{m}\dot{y}_i + d_{y,i} \\ \dfrac{\cos\phi_i\cos\theta_i}{m_i}U_{1a,i} - g - \dfrac{k_{z,i}}{m}\dot{z}_i + d_{z,i} \end{bmatrix}.$$

Thus the torque $U_{1,i}$ is calculated as

$$U_{1,i} = m_i\left\|\boldsymbol{a}_i - \hat{\boldsymbol{\sigma}}_{p,i} + \left[\frac{k_{x,i}}{m_i}\dot{x}_i, \frac{k_{y,i}}{m}\dot{y}_i, g + \frac{k_{z,i}}{m}\dot{z}_i\right]^T\right\|_2. \tag{12}$$

With $U_{1,i}$ solved, the actual linear acceleration $[\ddot{x}_i, \ddot{y}_i, \ddot{z}_i]^T$ can be calculated based on the dynamics model (1).

### 3.2. *Attitude control*

With $U_{1,i}$ solved, the desired angles are calculated from the following equations according to (1):

$$\begin{cases} \cos\phi_{d,i}\sin\theta_{d,i}\cos\psi_{d,i} + \sin\phi_{d,i}\sin\psi_{d,i} \\ \quad = \dfrac{m_i}{U_{1,i}}\left(\boldsymbol{a}_i(1) + \dfrac{k_{x,i}}{m_i}\dot{x}_i - \hat{\boldsymbol{\sigma}}_{p,i}(1)\right), \\ \cos\phi_{d,i}\sin\theta_{d,i}\sin\psi_{d,i} - \sin\phi_{d,i}\cos\psi_{d,i} \\ \quad = \dfrac{m_i}{U_{1,i}}\left(\boldsymbol{a}_i(2) + \dfrac{k_{y,i}}{m_i}\dot{y}_i - \hat{\boldsymbol{\sigma}}_{p,i}(2)\right), \\ \cos\phi_{d,i}\cos\theta_{d,i} \\ \quad = \dfrac{m_i}{U_{1,i}}\left(\boldsymbol{a}_i(3) + g + \dfrac{k_{z,i}}{m_i}\dot{z}_i - \hat{\boldsymbol{\sigma}}_{p,i}(3)\right). \end{cases} \tag{13}$$

Change $U_{1,i}$ into an extremely small value if $U_{1,i} = 0$, which is normally uncommon though.

Define the attitude error $\boldsymbol{e}_{a,i}$ and the vector $\boldsymbol{z}_{a,i}$ as

$$\boldsymbol{e}_{a,i} = \begin{bmatrix} \phi_i - \phi_{d,i} \\ \theta_i - \theta_{d,i} \\ \psi_i - \psi_{d,i} \end{bmatrix},$$

$$\boldsymbol{z}_{a,i} = \begin{bmatrix} \boldsymbol{e}_{a,i} \\ \dot{\boldsymbol{e}}_{a,i} \end{bmatrix},$$

whose derivative writes

$$\dot{\boldsymbol{z}}_{a,i} = \begin{bmatrix} \dot{\boldsymbol{e}}_{a,i} \\ \ddot{\boldsymbol{e}}_{a,i} \end{bmatrix} = \begin{bmatrix} \dot{\phi}_i - \dot{\phi}_{d,i} \\ \dot{\theta}_i - \dot{\theta}_{d,i} \\ \dot{\psi}_i - \dot{\psi}_{d,i} \\ \ddot{\phi}_i - \ddot{\phi}_{d,i} \\ \ddot{\theta}_i - \ddot{\theta}_{d,i} \\ \ddot{\psi}_i - \ddot{\psi}_{d,i} \end{bmatrix}$$

$$= \begin{bmatrix} \boldsymbol{w}_i - \boldsymbol{w}_{d,i} \\ \boldsymbol{h}_i - \boldsymbol{h}_{d,i} \end{bmatrix} + \begin{bmatrix} \mathbf{0} \\ \boldsymbol{\sigma}_{a,i} \end{bmatrix}, \tag{14}$$

where $\boldsymbol{w}_i$ and $\boldsymbol{h}_i$ are the angular velocity and acceleration of the $i$th UAV, respectively.

**Remark 3.3.** The changes in attitude angles of UAV are slowly-varying functions during the flight [20].

From Remark 3.3, $\boldsymbol{w}_{d,i}$ and $\boldsymbol{h}_{d,i}$ are approximately $\mathbf{0}$. Then (14) approximately equals to

$$\dot{\boldsymbol{z}}_{a,i} = \begin{bmatrix} \dot{\boldsymbol{e}}_{a,i} \\ \ddot{\boldsymbol{e}}_{a,i} \end{bmatrix} \approx \begin{bmatrix} \boldsymbol{w}_i \\ \boldsymbol{h}_i \end{bmatrix} + \begin{bmatrix} \mathbf{0} \\ \boldsymbol{\sigma}_{a,i} \end{bmatrix}. \tag{15}$$

Similarly, the total uncertainty term $\boldsymbol{\sigma}_{a,i}$ is estimated through ESO as follows.

For attitude control layer, define the observed states as

$$\begin{aligned}
\boldsymbol{v}_{1,i} &= [\phi_i \quad \theta_i \quad \psi_i]^T, \\
\boldsymbol{v}_{2,i} &= [\dot{\phi}_i \quad \dot{\theta}_i \quad \dot{\psi}_i]^T, \\
\boldsymbol{v}_{3,i} &= \boldsymbol{\sigma}_{a,i} + \begin{bmatrix} \frac{J_{y,i}-J_{z,i}}{J_{x,i}}\dot{\theta}_i\dot{\psi}_i - \frac{k_{\phi,i}}{J_{x,i}}\dot{\phi}_i \\ \frac{J_{z,i}-J_{x,i}}{J_{y,i}}\dot{\phi}_i\dot{\psi}_i - \frac{k_{\theta,i}}{J_{y,i}}\dot{\theta}_i \\ \frac{J_{x,i}-J_{y,i}}{J_{z,i}}\dot{\theta}_i\dot{\phi}_i - \frac{k_{\psi,i}}{J_{z,i}}\dot{\psi}_i \end{bmatrix}.
\end{aligned} \tag{16}$$

The state equation of attitude layer can be obtained from (1):

$$\begin{cases} \dot{\boldsymbol{v}}_{1,i} = \boldsymbol{v}_{2,i}, \\ \dot{\boldsymbol{v}}_{2,i} = \begin{bmatrix} b_{\phi,i}U_{2,i} \\ b_{\theta,i}U_{3,i} \\ b_{\psi,i}U_{4,i} \end{bmatrix} + \boldsymbol{v}_{3,i}, \\ \dot{\boldsymbol{v}}_{3,i} = \boldsymbol{\rho}_{a,i}, \end{cases}$$

where $\boldsymbol{\rho}_{a,i}$ is the derivative of the uncertainty term including the known dynamics for the attitude layer. Let the input be $\boldsymbol{v}_{1,i} = [\phi_i, \theta_i, \psi_i]^T$. Define the following extended state observer:

$$\begin{cases} \dot{\hat{\boldsymbol{v}}}_{1,i} = \hat{\boldsymbol{v}}_{2,i} + \frac{\alpha_{1,i}}{\varepsilon_i}(\boldsymbol{v}_{1,i} - \hat{\boldsymbol{v}}_{1,i}), \\ \dot{\hat{\boldsymbol{v}}}_{2,i} = \begin{bmatrix} b_{\phi,i}U_{2,i} \\ b_{\theta,i}U_{3,i} \\ b_{\psi,i}U_{4,i} \end{bmatrix} + \hat{\boldsymbol{v}}_{3,i} + \frac{\alpha_{2,i}}{\varepsilon_i^2}(\boldsymbol{v}_{1,i} - \hat{\boldsymbol{v}}_{1,i}), \\ \dot{\hat{\boldsymbol{v}}}_{3,i} = \frac{\alpha_{3,i}}{\varepsilon_i^3}(\boldsymbol{v}_{1,i} - \hat{\boldsymbol{v}}_{1,i}), \end{cases}$$

where $\hat{\boldsymbol{v}}_{1,i}$, $\hat{\boldsymbol{v}}_{2,i}$ and $\hat{\boldsymbol{v}}_{3,i}$ are the estimates of attitude state variables $\phi_i, \theta_i, \psi_i$, their derivatives and the uncertainty term $\boldsymbol{v}_{3,i}$, respectively; $\alpha_{k,i}(k = 1, 2, 3)$ and $\varepsilon_i$ are the same as those of position layer.

The attitude error states and its dynamics follow that

$$\begin{aligned}
\dot{\boldsymbol{\varsigma}}_{a,i} &= \begin{bmatrix} \dot{\hat{\boldsymbol{v}}}_{1,i} - \dot{\boldsymbol{v}}_{1,i} \\ \dot{\hat{\boldsymbol{v}}}_{2,i} - \dot{\boldsymbol{v}}_{2,i} \\ \dot{\hat{\boldsymbol{v}}}_{3,i} - \dot{\boldsymbol{v}}_{3,i} \end{bmatrix} = \begin{bmatrix} -\frac{\alpha_{1,i}}{\varepsilon_i}I & I & \mathbf{0} \\ -\frac{\alpha_{2,i}}{\varepsilon_i^2}I & \mathbf{0} & I \\ -\frac{\alpha_{3,i}}{\varepsilon_i^3}I & \mathbf{0} & \mathbf{0} \end{bmatrix} \boldsymbol{\varsigma}_{a,i} + \begin{bmatrix} \mathbf{0} \\ \mathbf{0} \\ I \end{bmatrix} \boldsymbol{\rho}_{a,i} \\
&= G_{a,i}\boldsymbol{\varsigma}_{a,i} + H_{a,i}\boldsymbol{\rho}_{a,i},
\end{aligned} \tag{17}$$

where

$$G_{a,i} = \begin{bmatrix} -\frac{\alpha_{1,i}}{\varepsilon_i}I & I & \mathbf{0} \\ -\frac{\alpha_{2,i}}{\varepsilon_i^2}I & \mathbf{0} & I \\ -\frac{\alpha_{3,i}}{\varepsilon_i^3}I & \mathbf{0} & \mathbf{0} \end{bmatrix}, \quad \boldsymbol{\varsigma}_{a,i} = \begin{bmatrix} \hat{\boldsymbol{v}}_{1,i} - \boldsymbol{v}_{1,i} \\ \hat{\boldsymbol{v}}_{2,i} - \boldsymbol{v}_{2,i} \\ \hat{\boldsymbol{v}}_{3,i} - \boldsymbol{v}_{3,i} \end{bmatrix},$$

$$H_{a,i} = \begin{bmatrix} \mathbf{0} \\ \mathbf{0} \\ I \end{bmatrix}.$$

The matrix $G_{a,i}$ can also be Hurwitz through suitably choosing the parameters $\alpha_{1,i}$, $\alpha_{2,i}$, $\alpha_{3,i}$ and $\varepsilon_i$. Then based on Lemma 3.1 and Assumption 3.2, the extended state observer asymptotically converges to its true value, which guarantees

$$\lim_{t\to\infty} \hat{\boldsymbol{v}}_{3,i} = \boldsymbol{v}_{3,i}. \tag{18}$$

Then according to (16), the observed value and the known dynamics, the compensation term is

$$\hat{\boldsymbol{\sigma}}_{a,i} = \hat{\boldsymbol{v}}_{3,i} - \begin{bmatrix} \frac{J_{y,i}-J_{z,i}}{J_{x,i}}\dot{\theta}_i\dot{\psi}_i - \frac{k_{\phi,i}}{J_{x,i}}\dot{\phi}_i \\ \frac{J_{z,i}-J_{x,i}}{J_{y,i}}\dot{\phi}_i\dot{\psi}_i - \frac{k_{\theta,i}}{J_{y,i}}\dot{\theta}_i \\ \frac{J_{x,i}-J_{y,i}}{J_{z,i}}\dot{\theta}_i\dot{\phi}_i - \frac{k_{\psi,i}}{J_{z,i}}\dot{\psi}_i \end{bmatrix}.$$

Therefore with (18), define $\boldsymbol{\delta}_{a,i} = \boldsymbol{\sigma}_{a,i} - \hat{\boldsymbol{\sigma}}_{a,i}$ as the observed error vector. It satisfies

$$\lim_{t\to\infty} \|\boldsymbol{\delta}_{a,i}\| = 0. \tag{19}$$

Similar to position control (10), choose two suitable matrices $\bar{A}_0$, $\bar{A}_1 \in R^{3\times 3}$ and design the angular acceleration with ESO as

$$\boldsymbol{h}_i = -\bar{A}_1\dot{\boldsymbol{e}}_{a,i} - \bar{A}_0\boldsymbol{e}_{a,i} - \hat{\boldsymbol{\sigma}}_{a,i}. \tag{20}$$

The system (15) is transformed into

$$\dot{\boldsymbol{z}}_{a,i} = \begin{bmatrix} \mathbf{0} & I \\ -\bar{A}_0 & -\bar{A}_1 \end{bmatrix} \begin{bmatrix} \boldsymbol{e}_{a,i} \\ \dot{\boldsymbol{e}}_{a,i} \end{bmatrix} + \begin{bmatrix} \mathbf{0} \\ \boldsymbol{\delta}_{a,i} \end{bmatrix}, \tag{21}$$

where the coefficient matrix can be Hurwitz by suitably choosing $\bar{A}_0$ and $\bar{A}_1$. From dynamics (1), the angular acceleration $\boldsymbol{h}_i$ satisfies the constraint that

$$\boldsymbol{h}_i = \begin{bmatrix} \frac{J_{y,i}-J_{z,i}}{J_{x,i}}\dot{\theta}_i\dot{\psi}_i + \frac{U_{2a,i}}{J_{x,i}}d_i - \frac{k_{\phi,i}}{J_{x,i}}\dot{\phi}_i + d_{\phi,i} \\ \frac{J_{z,i}-J_{x,i}}{J_{y,i}}\dot{\phi}_i\dot{\psi}_i + \frac{U_{3a,i}}{J_{y,i}}d_i - \frac{k_{\theta,i}}{J_{y,i}}\dot{\theta}_i + d_{\theta,i} \\ \frac{J_{x,i}-J_{y,i}}{J_{z,i}}\dot{\theta}_i\dot{\phi}_i + \frac{U_{4a,i}}{J_{z,i}} - \frac{k_{\psi,i}}{J_{z,i}}\dot{\psi}_i + d_{\psi,i} \end{bmatrix}.$$

Then the control inputs $U_{k,i}(k=2,3,4)$ are solved as

$$\begin{aligned} U_{2,i} &= \frac{J_{x,i}}{d_i}\left(\boldsymbol{h}_i(1) - \frac{J_{y,i}-J_{z,i}}{J_{x,i}}\dot{\theta}_i\dot{\psi}_i + \frac{k_{\phi,i}}{J_{x,i}}\dot{\phi}_i - \hat{\boldsymbol{\sigma}}_{a,i}(1)\right), \\ U_{3,i} &= \frac{J_{y,i}}{d_i}\left(\boldsymbol{h}_i(2) - \frac{J_{z,i}-J_{x,i}}{J_{y,i}}\dot{\phi}_i\dot{\psi}_i + \frac{k_{\theta,i}}{J_{y,i}}\dot{\theta}_i - \hat{\boldsymbol{\sigma}}_{a,i}(2)\right), \\ U_{4,i} &= J_{z,i}\left(\boldsymbol{h}_i(3) - \frac{J_{x,i}-J_{y,i}}{J_{z,i}}\dot{\theta}_i\dot{\phi}_i + \frac{k_{\psi,i}}{J_{z,i}}\dot{\psi}_i - \hat{\boldsymbol{\sigma}}_{a,i}(3)\right). \end{aligned} \tag{22}$$

With $U_{k,i}(k=2,3,4)$ obtained, the actual angular acceleration $[\ddot{\phi}_i, \ddot{\theta}_i, \ddot{\psi}_i]^T$ can be calculated based on the dynamics model (1).

### 3.3. *System robustness analysis*

Combining the FAS control and ESO compensation, the accelerations designed for position and attitude layers are recalled as

$$\boldsymbol{a}_i = \boldsymbol{a}_j - A_1\dot{\boldsymbol{e}}_{p,i} - A_0\boldsymbol{e}_{p,i} - \hat{\boldsymbol{\sigma}}_{p,i}, \tag{23}$$

$$\boldsymbol{h}_i = -\bar{A}_1\dot{\boldsymbol{e}}_{a,i} - \bar{A}_0\boldsymbol{e}_{a,i} - \hat{\boldsymbol{\sigma}}_{a,i}. \tag{24}$$

And the corresponding systems are

$$\dot{\boldsymbol{z}}_{p,i} = \begin{bmatrix} \mathbf{0} & I \\ -A_0 & -A_1 \end{bmatrix}\begin{bmatrix} \boldsymbol{e}_{p,i} \\ \dot{\boldsymbol{e}}_{p,i} \end{bmatrix} + \begin{bmatrix} \mathbf{0} \\ \boldsymbol{\delta}_{p,i} \end{bmatrix}, \tag{25}$$

$$\dot{\boldsymbol{z}}_{a,i} = \begin{bmatrix} \mathbf{0} & I \\ -\bar{A}_0 & -\bar{A}_1 \end{bmatrix}\begin{bmatrix} \boldsymbol{e}_{a,i} \\ \dot{\boldsymbol{e}}_{a,i} \end{bmatrix} + \begin{bmatrix} \mathbf{0} \\ \boldsymbol{\delta}_{a,i} \end{bmatrix}. \tag{26}$$

With (9) and (19), the system response output is bounded based on BIBO stable criterion [21]. Moreover, define

$$\boldsymbol{z}_i = \begin{bmatrix} \boldsymbol{z}_{p,i} \\ \boldsymbol{z}_{a,i} \end{bmatrix}. \tag{27}$$

The derivative of $z_i$ is

$$\dot{\boldsymbol{z}} = \begin{bmatrix} \dot{\boldsymbol{z}}_{p,i} \\ \dot{\boldsymbol{z}}_{a,i} \end{bmatrix} = A^*\boldsymbol{z} + B^*\boldsymbol{u}^*, \tag{28}$$

where

$$A^* = \begin{bmatrix} \mathbf{0} \quad I & \mathbf{0} \\ -A_0 \quad -A_1 & \mathbf{0} \quad I \\ \mathbf{0} & -\bar{A}_0 \quad -\bar{A}_1 \end{bmatrix},$$

$$B^* = \begin{bmatrix} \mathbf{0} & \mathbf{0} \\ I & \mathbf{0} \\ \mathbf{0} & \mathbf{0} \\ \mathbf{0} & I \end{bmatrix}, \quad \boldsymbol{u}^* = \begin{bmatrix} \boldsymbol{\delta}_{p,i} \\ \boldsymbol{\delta}_{a,i} \end{bmatrix}.$$

From (9) and (19), we can conclude that

$$\lim_{t\to\infty}\|B^*\boldsymbol{u}^*\| = 0. \tag{29}$$

The solution of linear time-invariant system (28) is given by

$$\boldsymbol{z}(t) = e^{A^*(t-t_0)}\boldsymbol{z}(t_0) + \int_{t_0}^{t} e^{A^*(t-\tau)}B^*\boldsymbol{u}^*(\tau)d\tau.$$

Since matrix $A^*$ is Hurwitz, it satisfies

$$\|e^{A^*(t-t_0)}\| \le ke^{-\lambda(t-t_0).} \tag{30}$$

With (30), one can conclude that

$$\begin{aligned} \|\boldsymbol{z}(t)\| &\le ke^{-\lambda(t-t_0)}\|\boldsymbol{z}(t_0)\| + \int_{t_0}^{t} ke^{-\lambda(t-\tau)}\|B^*\| \\ &\quad \times \|\boldsymbol{u}^*(\tau)\|d\tau \\ &\le ke^{-\lambda(t-t_0)}\|\boldsymbol{z}(t_0)\| \\ &\quad + \frac{k}{\lambda}(1-e^{-\lambda(t-t_0)})\|B^*\| \sup_{t_0\le\tau\le t}\|\boldsymbol{u}^*(\tau)\| \\ &\le ke^{-\lambda(t-t_0)}\|\boldsymbol{z}(t_0)\| + \frac{k}{\lambda}\|B^*\| \sup_{t_0\le\tau\le t}\|\boldsymbol{u}^*(\tau)\|. \end{aligned}$$

So considering (29), the system (28) is input-to-state stable (ISS).

### 3.4. *System stability analysis*

Considering position and attitude layers together, define

$$\varsigma_i = \begin{bmatrix} \varsigma_{p,i} \\ \varsigma_{a,i} \end{bmatrix}, \quad G_i = \begin{bmatrix} G_{p,i} & \mathbf{0} \\ \mathbf{0} & G_{a,i} \end{bmatrix},$$

$$\boldsymbol{\rho}_i = \begin{bmatrix} \boldsymbol{\rho}_{p,i} \\ \boldsymbol{\rho}_{a,i} \end{bmatrix}, \quad H_i = \begin{bmatrix} H_{p,i} & \mathbf{0} \\ \mathbf{0} & H_{a,i} \end{bmatrix}.$$

**Theorem 3.4.** *Consider the system (1) with the FAS-ESO. The designed control laws (23) and (24) guarantee that the error state $\boldsymbol{z}_i$ converges into the following ellipsoid centered at the origin:*

$$\Theta_{\epsilon_i,\kappa_i}(0) = \left\{\boldsymbol{z}_i \,\middle|\, \frac{1}{2}\boldsymbol{z}_i^T P_i \boldsymbol{z}_i \le \frac{\epsilon_i}{\kappa_i}\right\},$$

*where $\epsilon_i$ and $\kappa_i$ are given in the following proof.*

The proofs stability of the system and convergence of the state are as follows.

**Proof.** (1) Stability of the closed-loop system

From (7), (17), (25), and (26), the closed-loop system can be presented as

$$\begin{bmatrix} \dot{\boldsymbol{z}}_i \\ \dot{\varsigma}_i \end{bmatrix} = \begin{bmatrix} A^* & \mathbf{0} \\ \mathbf{0} & G_i \end{bmatrix}\begin{bmatrix} \boldsymbol{z}_i \\ \varsigma_i \end{bmatrix} + \begin{bmatrix} B^*\boldsymbol{u}^* \\ H_i\boldsymbol{\rho}_i \end{bmatrix}. \tag{31}$$

It is obvious that the eigenvalues satisfy

$$\operatorname{eig}\left(\begin{bmatrix} A^* & \mathbf{0} \\ \mathbf{0} & G_i \end{bmatrix}\right) = \operatorname{eig}(A^*) \cup \operatorname{eig}(G_i).$$

Since $A^*$ and $G_i$ can be Hurwitz and with the condition (29), the nontrivial condition on the system (31) is the boundedness of $\boldsymbol{\rho}_i$. This means that the generalized uncertainty term must be differentiable, which is a reasonable assumption. □

**Proof.** (2) Convergence of $\boldsymbol{z}_i$

According to [22], let $A^* \in R^{n\times n}$ satisfy

$$\mathrm{Re}\lambda_k(A^*) \leq -\frac{\xi_i}{2}, \quad k = 1, 2, \ldots, n,$$

where $\xi_i > 0$, and then there exists a positive definite matrix $P_i \in R^{n\times n}$ satisfying

$$A^{*T}P_i + P_iA^* \leq -\xi_i P_i.$$

Consider the following Lyapunov function:

$$V_i = \frac{1}{2}\boldsymbol{z}_i^T P_i \boldsymbol{z}_i.$$

The time derivative of $V_i$ is

$$\begin{aligned}
V_i &= \frac{1}{2}\dot{\boldsymbol{z}}_i^T P_i \boldsymbol{z}_i + \frac{1}{2}\boldsymbol{z}_i^T P_i \dot{\boldsymbol{z}}_i \\
&= \frac{1}{2}(A^*\boldsymbol{z}_i + B^*\boldsymbol{u}^*)^T P_i \boldsymbol{z}_i + \frac{1}{2}\boldsymbol{z}_i^T P_i (A^*\boldsymbol{z}_i + B^*\boldsymbol{u}^*) \\
&= \frac{1}{2}\boldsymbol{z}_i^T (A^{*T}P_i + P_iA^*)\boldsymbol{z}_i + \boldsymbol{z}_i^T P_i B^*\boldsymbol{u}^* \\
&\leq -\frac{\xi_i}{2}\boldsymbol{z}_i^T P_i \boldsymbol{z}_i + \|\boldsymbol{z}_i\| \cdot \|P_i\| \cdot \|B^*\boldsymbol{u}^*\| \\
&\leq -\frac{\xi_i}{2}\boldsymbol{z}_i^T P_i \boldsymbol{z}_i + \frac{\eta_i}{2}\|\boldsymbol{z}_i\|^2 + \frac{1}{2\eta_i}\|P_i\|^2 \cdot \|B^*\boldsymbol{u}^*\|^2 \\
&\leq -\frac{1}{2}\boldsymbol{z}_i^T (\xi_i P_i - \eta_i I)\boldsymbol{z}_i + \frac{1}{2\eta_i}\|P_i\|^2 \cdot \|B^*\boldsymbol{u}^*\|^2 \\
&\leq -\frac{\lambda_{\min}(\xi_i P_i - \eta_i I)}{\lambda_{\max}(P_i)} V_i + \frac{1}{2\eta_i}\|P_i\|^2 \cdot \|B^*\boldsymbol{u}^*\|^2 \\
&\leq -\kappa_i V_i + \epsilon_i, 
\end{aligned} \tag{32}$$

where

$$\kappa_i = \frac{\lambda_{\min}(\xi_i P_i - \eta_i I)}{\lambda_{\max}(P_i)}, \epsilon_i = \frac{1}{2\eta_i}\|P_i\|^2 \cdot \|B^*\boldsymbol{u}^*\|^2.$$

It thus follows from the comparison lemma that

$$V_i \leq V_i(0)e^{-\kappa_i t} + \frac{\epsilon_i}{\kappa_i}(1 - e^{-\kappa_i t}),$$

which gives

$$V_i \leq \left(V_i(0) - \frac{\epsilon_i}{\kappa_i}\right)e^{-\kappa_i t} + \frac{\epsilon_i}{\kappa_i} \to \frac{\epsilon_i}{\kappa_i}, \; t \to \infty.$$

Thus, the state $\boldsymbol{z}_i$ eventually converges into the ellipsoid $\Theta_{\epsilon_i,\kappa_i}(0)$ in Theorem 3.4. This completes the proof. □

It is worth noting that the system will not be stable or the state $\boldsymbol{z}_i$ cannot converge to the neighborhood of the origin without ESO. Since the input $\boldsymbol{u}^*$ in (28) will be the uncertainty $[\boldsymbol{\sigma}_{p,i}, \quad \boldsymbol{\sigma}_{a,i}]^T$ instead of the observed error $[\boldsymbol{\delta}_{p,i}, \quad \boldsymbol{\delta}_{a,i}]^T$ which is in the neighborhood of zero as in (9) and (19), the convergence of the system (31) would no longer hold due to the unknown value of the uncertainty. Also, $\epsilon_i$ in (32) containing the input $\boldsymbol{u}^*$ with uncertainty may be not an extremely small value, which cannot support the convergence proof of the state $\boldsymbol{z}_i$. Thanks to the convergence of the ESO, the uncertainty estimation error $[\boldsymbol{\delta}_{p,i}, \quad \boldsymbol{\delta}_{a,i}]^T$ tends to 0 as $t \to \infty$. As a result, the ultimate convergence of (27) and (31) can be guaranteed.

## 4. Examples

The results of the proposed method are compared with a recent nonsingular fast terminal sliding mode control (SMC) method in [23]. Consider a UAV team with four agents and one virtual leader. Parameters related to the dynamics model of the four UAVs are shown in Table 1.

The extended state observer parameters are set as

$$\varepsilon_i = 1.2, \quad \alpha_{1,i} = 9, \quad \alpha_{2,i} = 22, \quad \alpha_{3,i} = 16 \; (i = 1, \ldots, 4).$$

The control parameters are designed as in Table 2.

The formation in this example is maintained on a horizontal plane, and the communication topology is shown in Fig. 5.

Let the virtual leader's trajectory be

$$p_0 = \begin{bmatrix} 2.5\cos(0.4t) \\ 2.5\sin(0.4t) \\ 0.5t + 5 \end{bmatrix}.$$

The initial positions of UAV are listed in Table 3. The initial attitudes are $[0, 0, 0]^T$.

The UAVs are subject to disturbances $d_k(k = x, y, z, \phi, \theta, \psi)$ after $t = 30$ s which are modeled as

$$\begin{aligned}
d_{x,y,z} &= 2.5(e^{\sin(0.1t+\frac{\pi}{5})} - e^{\cos(0.1t-\frac{\pi}{5})}) \\
&\quad - 0.5\sin(0.1t) + 0.5\cos(0.1t), \\
d_{\phi,\theta,\psi} &= 0.5\sin(0.1t).
\end{aligned}$$

The actuator faults $f_{r,i}$ $(r, i = 1, 2, 3, 4)$ occur after $t = 60$ s governed by the fault functions

$$f_1 = -1.5,$$
$$f_{2,3,4} = 0.5\sin(0.1t).$$

Table 1. Formation parameters.

| Parameter | Value |
|---|---|
| $m$ | 2 kg |
| $g$ | $9.81\ \mathrm{m/s^2}$ |
| $k_{x,y,z}$ | 0.01 kg/s |
| $k_{\phi,\theta,\psi}$ | $1.49 \times 10^{-7}\ \mathrm{N \cdot s/rad}$ |
| $J_{x,y,z}$ | $1.25\ \mathrm{N \cdot s^2/rad}$ |
| $d$ | 0.3 m |

Table 2. FAS parameters.

| $A_0$ | $A_1$ | $\bar{A}_0$ | $\bar{A}_1$ |
|---|---|---|---|
| $6.25I$ | $5I$ | $36I$ | $12I$ |

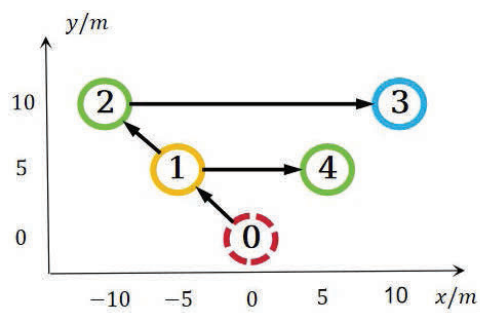


Fig. 5. Horizontal plane shape with communication topology.

We define the loss function as $\mathrm{loss}_i = \|\boldsymbol{e}_{p,i}\|_2$ to quantify the error of both controllers. Define loss function as $E_k = \|\boldsymbol{\delta}_{k,i}\|_2$, $(k = a, p)$ to quantify the error of the extended state observer in position and attitude layers respectively. Additionally, we calculate the sum of the loss function $\mathrm{loss}_i$ with ESO or without to illustrate its effect.

Taking the position $x$ and the roll angle $\phi$ as examples, the observation results of the extended state observer are shown in Fig. 6. Both the estimation errors in position and attitude layers are shown in Fig. 7. The sum of loss values with or without ESO in 80 s is in Table 4.

It can be seen that the observations of the extended state observer are able to converge to the true values with small error fluctuations in a finite time when disturbances or faults are added. And the errors are decreased with ESO.

(1) Results of position control

The trajectories in this example are shown in Fig. 8. The loss functions of both methods are compared in Fig. 9. Figure 10 shows the formation shape and its projection to the horizontal plane at the 80th second.

Table 3. Initial positions.

| UAV | $x[m]$ | $y[m]$ | $z[m]$ |
|---|---|---|---|
| 0 | 2.5 | 0 | 5 |
| 1 | −1 | 1 | 4 |
| 2 | −1 | −1 | 4 |
| 3 | 1 | 1 | 4 |
| 4 | 1 | −1 | 4 |

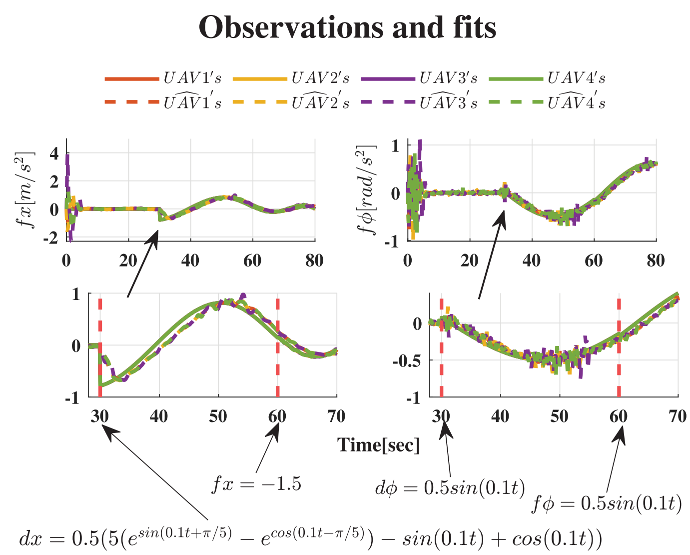


Fig. 6. Observed versus true values of the total uncertainties.

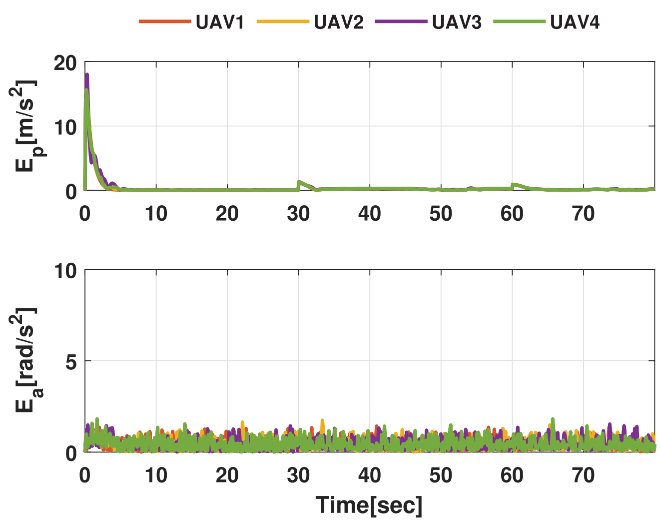


Fig. 7. The estimation errors in position and attitude layers.

It can be seen that the proposed method results in higher convergence rate and smaller steady errors.

Table 4. The sum of loss function ([$m$]).

| Algorithm | UAV1 | UAV2 | UAV3 | UAV4 |
|---|---|---|---|---|
| FAS-ESO | 144.2894 | 151.6355 | 222.7442 | 165.1304 |
| FAS | 175.2373 | 193.1059 | 273.9323 | 186.3116 |

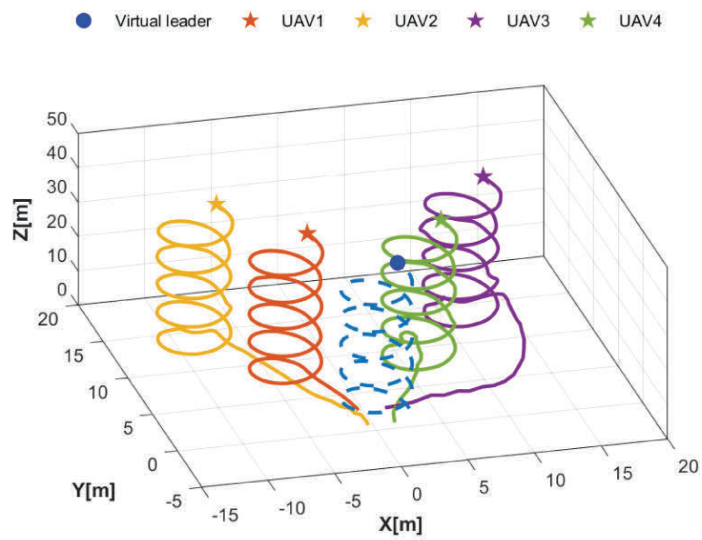


Fig. 8. Formation flight trajectories.

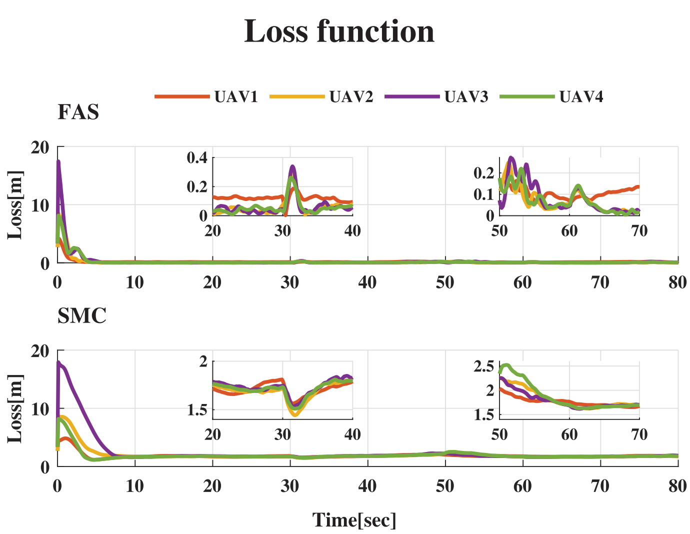


Fig. 9. Loss function of both methods.

(2) Results of attitude control

Figure 11 illustrates the consistency of attitude angles under FAS.

From Fig. 11, one can conclude that the proposed scheme basically meets the attitude requirements.

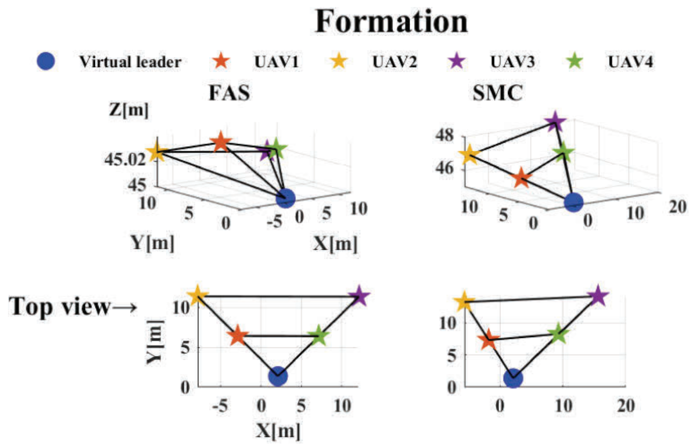


Fig. 10. Three-dimensional and top-down view of the formation.

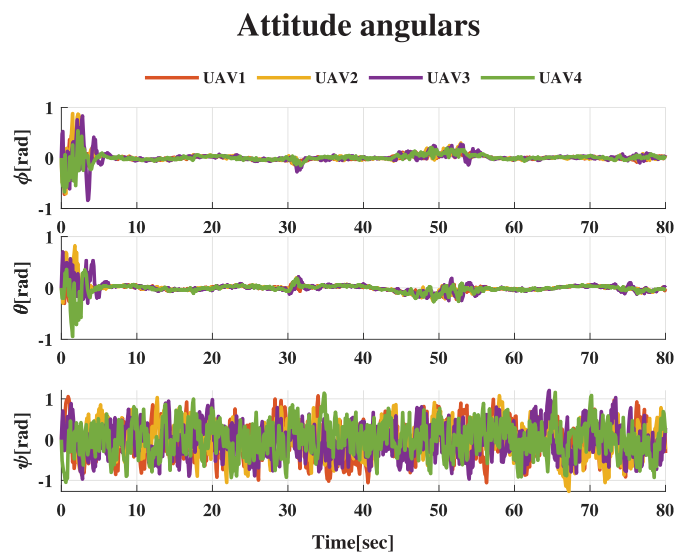


Fig. 11. Atitudes control curves.

## 5. Conclusion

In this paper, we consider the formation control of UAVs with both external disturbances and actuator faults. A fully actuated system control scheme is designed to drive the UAV formation to travel along the desired trajectory. An extended state observer is designed to estimate uncertainties, which is used to compensate the effects of disturbances and faults in the controller. In order to demonstrate the effectiveness of the proposed algorithm, extensive numerical experiments are conducted in comparison with a recent SMC method. The results confirm the convergence of the uncertainty estimation by the ESO and the FAS algorithm performs well both in position and attitude control. Overall, FAS achieves accurate and fast tracking of formation trajectory with little fluctuation, small steady-state errors and well formation maintenance. Control efforts will be devoted to techniques for obstacle avoidance and navigation.

**Acknowledgments**

This work was supported in part by the National Natural Science Foundation (NNSF) of China (Grant 62303133, 62188101) and in part by the Guangdong Basic and Applied Basic Research Foundation (Grant 2022A1515011274).

**ORCID**

Zhihao Liu https://orcid.org/0009-0000-0751-1557
Peng Li https://orcid.org/0000-0002-8217-1326

## References

[1] J. Wang, W. B. Gu and L. Y. Dou, Leader-Follower formation control of multiple UAVs with trajectory tracking design, *Acta Aeronaut. Astronaut. Sin.* **41**(S1) (2020) 88–98.
[2] W. W. Pan, D. P. Jiang, Y. J. Pang *et al.*, A multi-AUV formation algorithm combining artificial potential field and virtual structure, *Binggong Xuebao/Acta Armament.* **38**(2) (2017) 326–334.
[3] Q. Luo and H. Duan, Distributed UAV flocking control based on homing pigeon hierarchical strategies, *Aerosp. Sci. Technol.* **70** (2017) 257–264.
[4] M. Yang, Y. Shou, Y. Tang, C. Liu and B. Xu, Multi-quadrotor UAVs formation maintenance and collision avoidance control, *Aerosp. Sci. Technol.* **43**(S1) (2020) 89–99.
[5] Q. Wei, R. Liu and H. Zhang, High-order consistent formation control method for quadrotor UAV, *Electro-Opt. Control* **26**(8) (2019) 1–5.
[6] B. Yu, X. Dong, S. Zongying *et al.*, Formation control for quadrotor swarm systems: Algorithms and experiments, in *Proc. 32nd Chinese Control Conf.* (IEEE, 2013), pp. 7099–7104.
[7] X. Dong, B. Yu, Z. Shi and Y. Zhong, Time varying formation control for unmanned aerial vehicles: Theories and applications, *IEEE Trans. Control Syst. Technol.* **23**(1) (2014) 340–348.
[8] H. Wang, B. Zheng, S. Lu *et al.*, Adaptive fault-tolerant control of UAV formation based on observer, *Electron. Measur. Technol.* **45**(17) (2022) 56–64.
[9] D. Zhang, T. Liu and J. Song, Optimal cooperative fault-tolerant control of UAV formation based on dynamic programming, *Electro-Opt. Control* **30**(4) (2023) 34–39.
[10] L. Dou, T. Chen and Q. Mao, Distributed quadrotor formation tracking control based on a disturbance observer, *J. Tianjin Univ. (Natural Sci. Eng. Technol. Edition)* **51**(8) (2018) 817–824.
[11] G.-R. Duan, High-order system approaches: I. Fully actuated systems and parametric design, *Acta Automat. Sin.* **46**(7) (2020) 1333–1345.
[12] H. Sun, Research on trajectory tracking control of six-degree-of-freedom manipulator based on high-order fully actuated system model, *Harbin Univ. Sci. Technol.* (2023), doi: 10.27063/d.cnki.ghlgu.2023.000814.
[13] T. Zhao and G. Duan, Fully actuated system approach to attitude control of flexible spacecraft with nonlinear time-varying inertia, *Sci. China (Inform. Sci.)* **65**(11) (2022) 148–162.
[14] Z. Qin and G. D. Ren, Fully actuated system approach for 6DOF spacecraft control based on extended state observer, *J. Syst. Sci. Complex.* **35**(2) (2022) 604–622.
[15] Z. Liu and P. Li, Robust multi-mobile robot formation control: A fully actuated system control approach, *2024 3rd Conf. Fully Actuated System Theory and Applications (FASTA)* (IEEE, 2024), pp. 1011–1016.
[16] Y. Fei, Y. Sun and P. Shi, Robust hierarchical formation control of unmanned aerial vehicles via neural-based observers, *Drones* **6**(2) (2022) 1119–1125.
[17] W. Jun and L. Ang, Multi-quadrotor UAV formation adaptive fault-tolerant control, *J. Lanzhou Univ. Technol.* **50**(04) (2024) 69–76.
[18] J. Wang and M. Luo, Robust global fast terminal sliding mode formation fault-tolerant control of multi-quadrotor UAV, *Flight Mech.* **42**(03) (2024) 68–75+88.
[19] W. Zhang, J. Ma and K. Xing, State feedback control of interference mismatched discrete systems based on a generalized expansion state observer, *Control Decis. Making* **31**(6) (2016) 1128–1132.
[20] D. Qingfeng, J. Wuxing, G. Changsheng and A. Mingruo, Dual-loop control of metamorphic centroid quadrotor UAV considering the dynamic characteristics of the slider, *J. Beijing Univ. Aeronaut. Astronaut.* **50**(3) (2024) 861–873.
[21] J. P. Hespanha, *Linear Systems Theory*, 2nd edn. (Princeton University Press, 2018).
[22] G. R. Duan, High-order fully actuated system approaches: Part III. Robust control and high-order backstepping, *Int. J. Syst. Sci.* **52**(5) (2021) 952–971.
[23] H. Yulong, S. Wei, C. Baoshan, G. Xiaolin and L. Guoqiang, Study on nonsingular fast terminal sliding mode control, *Syst. Eng. Electron.* **39** (2017) 1119–1125.